# A Computational Study of Multicomponent Orbital Interactions during the Cyclization of Silyl, Germyl, and Stannyl Radicals onto C−N and C−O Multiple Bonds

Uta Wille,* Jeremy C.-S. Tan, and Eva-Katrin Mucke

ARC Centre of Excellence for Free Radical Chemistry and Biotechnology, School of Chemistry/BIO21 Molecular Science and Biotechnology Institute, The University of Melbourne, 30 Flemington Road, Parkville, Victoria 3010, Australia

uwille@unimelb.edu.au
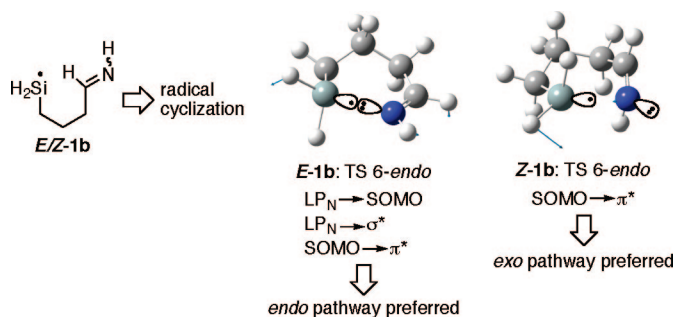
BHandHLYP/6-311G** and BHandHLYP/DZP computations of the potential surface of Si-, Ge-, and Sn-radical cyclizations onto the imine double bond reveal that these reactions proceed through simultaneous $SOMO \rightarrow \pi^*$, $LP_N \rightarrow SOMO$, and $LP_N \rightarrow \sigma^*$ interactions. Such multicomponent orbital interactions are responsible for the regioselectivity in these radical cyclizations, where the nucleophilic radical unexpectedly attacks the more electron-rich end of the π system. Less nucleophilic heteroatoms, for example, the nitrogen atom in nitriles or the oxygen atom in carbonyl compounds, show reduced LP interactions with the radical center in the respective transition states, so that these reactions predominantly occur in the "classical" fashion and with the expected regioselectivities of nucleophilic radicals through $SOMO \rightarrow \pi^*$ interactions. This supports the hypothesis that Si-, Ge- and, to a lesser extent, Sn-radicals are ambiphilic in nature and that the unpaired electron is not necessarily the most reactive site in a radical but can act as an observer of a nucleophilic attack at the radical center.

Introduction

The formation of carbon−heteroatom and heteroatom−heteroatom bonds are central goals in synthetic organic chemistry. Radical additions and cyclizations onto π systems are a very efficient methodology to achieve this goal under usually mild conditions and with high tolerance toward functional groups.[1] It is generally believed that the primary orbital interactions in radical additions to π systems are $SOMO \rightarrow \pi$ (= HOMO) for electrophilic radicals and $SOMO \rightarrow \pi^*$ (= LUMO) for nucleophilic radicals, respectively.[2] Whereas this appears to be the case for nucleophilic C-centered alkyl and electrophilic O-centered alkoxyl radicals,

whose intramolecular homolytic addition reactions are governed by Beckwith−Houk considerations,[3,4] we have recently found that acyl and silyl radicals, which are commonly considered as nucleophilic species, undergo addition to the C=N double bond in imines with high preference at the more electron-rich nitrogen end.[5,6] In the case of the addition of $H_3Si^{\bullet}$ to methaneimine (CH_2=NH), preliminary computational investigations concluded that this outcome is the result of simultaneous interactions in the transition state between (a) the radical SOMO with the imine

(1) Renaud, P.; Sibi, M. P. *Radicals in Organic Synthesis*; Wiley-VCH: Weinheim, 2001; Vols. *1, 2*.

(2) Fossey, J.; Lefort, D.; Sorba, J. *Free Radicals in Organic Chemistry*; John Wiley & Sons−Masson: Chichester, 1995.

(3) (a) Beckwith, A. L. J.; Schiesser, C. H. *Tetrahedron* **1985**, *41*, 3925. (b) Spellmeyer, D. C.; Houk, K. N. *J. Org. Chem.* **1987**, *52*, 959.

(4) Hartung, J.; Gallou, F. *J. Org. Chem.* **1995**, *60*, 6706.

(5) Schiesser, C. H.; Matsubara, H.; Ritsner, I.; Wille, U. *Chem. Commun.* **2006**, 1067.

(6) Schiesser, C. H.; Wille, U.; Matsubara, H.; Ryu, I. *Acc. Chem. Res.* **2007**, *40*, 303.
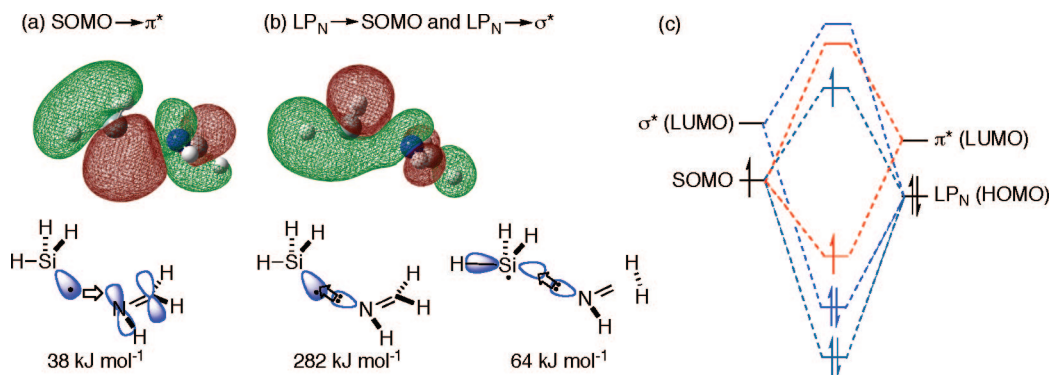
FIGURE 1. Transition state for the homolytic addition of $H_3Si^{\bullet}$ to the nitrogen end in imine: (a, b) BHandHLYP/6-311G** optimized Kohn−Sham orbitals; (c) energy profile diagram for NBO analysis of orbital interactions.

π^* orbital (calculated to be the LUMO), SOMO $\rightarrow \pi^*$, and (b) the lone pair of electrons at nitrogen, LP_N (calculated to be the HOMO of the π system), with a Si−H σ^* orbital (calculated to be the radical LUMO), $LP_N \rightarrow \sigma^*$, which are operating between the two reacting units.[5–7] Natural Bond Orbital (NBO) analysis at the BHandHLYP/6-311G** level of theory revealed that the SOMO $\rightarrow \pi^*$ interaction found in the α spin set is worth 38 kJ mol^{-1}. In both the α and β spin set a $LP_N \rightarrow \sigma^*$ interaction, worth a total of 64 kJ mol^{-1}, is occurring. Most importantly, however, the β spin set revealed a third interaction between LP_N and SOMO ($LP_N \rightarrow$ SOMO), which is worth 282 kJ mol^{-1}. Thus, the orbital interactions resulting from nucleophilic attack of the imine nitrogen at the radical center, e.g., $LP_N \rightarrow$ SOMO and $LP_N \rightarrow \sigma^*$, comprise 90% of the total interactions in the transition state, leaving only 10% for the "classical" radical addition pathway expected for a nucleophilic radical through SOMO $\rightarrow \pi^*$ interaction. Visualization of the Kohn−Sham orbitals generated at the same level of theory shows the overlap of the two reacting units in this transition state (Figure 1a,b), and an energy profile diagram illustrating the different orbital interactions is shown in Figure 1c. It is the dominating nucleophilic interaction of the imine nitrogen with the radical center in the transition state that accounts for the unexpected regioselectivity in this addition. This clearly shows that Si-radicals are ambiphilic in nature.[8]

As a consequence of this finding, we became interested whether and how such multicomponent orbital interactions may influence the regioselectivity in cyclizations of Si-radicals and higher main-group IV centered radicals, namely, Ge- and Sn-radicals, onto polarized π systems, such as C=N, C≡N and C=O bonds.[9] In this paper, we report full details of this computational investigation and show how the availability of a lone pair at the heteroatom in the imine, nitrile, and carbonyl moiety determines whether the radicals are reacting as nucleophilic or electrophilic species.

Computational Methods

The calculations were carried out using the Gaussian 03 program.[10] Geometry optimizations were performed using the hybrid density functional method BHandHLYP/6-311G** for Si- and Ge-centered radicals. The reactions involving Sn-centered radicals were performed using BHandHLYP in combination with a (valence) double-ζ pseudopotential (DZP) basis set[11] for tin and the 6-311G** basis set for C, N, O, and H. The ground and transition states were verified by vibrational frequency analysis at the same levels of theory, and all identified transition states showed only one imaginary frequency. The spin expectation value, $<s^2>$, was in all cases very close to 0.75 after spin annihilation. The NBO analyses of the transition states were carried out with NBO 5.0,[12] linked through the Gaussian program and were performed at the same level of theory as the geometry optimization, using the choose option to define bonds and lone pairs of electrons. The calculations were benchmarked by computing the potential surface of the addition of $H_3Si^{\bullet}$ to the nitrogen end in $CH_2=NH$ using various ab initio and hybrid density functional methods, e.g., (U)HF/6-311G**, MP2/6-311G**, G3MP2, QCISD/cc-pVDZ, CCSD(T)/cc-pVDZ// BHandHLYP/aug-cc-pVTZ (single point energy calculations), B3LYP/6-311G**, and BHandHLYP in combination with the 6-311G**, cc-pVDZ, aug-cc-pVDZ, cc-pVTZ, and aug-cc-pVTZ basis sets. This procedure revealed that the energies and geometries computed with high-level ab initio methods such as QCISD, CCSD(T), and G3MP2 were similar to those obtained with the low-cost BHandHLYP/6-311G** method, which is consistent with

(7) Wille, U.; Mucke, E.-K. *Chem. Lett.* **2007**, *36*, 300.

(8) The first reported 5-*endo-dig* cyclization onto a C≡C triple bond involving a silyl radical (Amrein, S.; Studer, A. *Chem. Commun.* **2002**, 1592.) is suggested to also involve multicomponent orbital interactions; see ref 5.

(9) Selected overviews on Si-, Ge-, and Sn-radical chemistry: (a) Chatgilialoglu, C. *Organosilanes in Radical Chemistry*; John Wiley & Sons: Hoboken, NJ, 2004. (b) Lee, V. Y.; Sekiguchi, A. *Eur. J. Inorg. Chem.* **2005**, 1209. (c) Taraban, M. B.; Volkova, O. S.; Kruppa, A. I.; Leshina, T. V. In *Chemistry of Organic Germanium, Tin and Lead Compounds*; Rappoport, Z., Ed.; John Wiley & Sons: Hoboken, NJ, 2003; Vol. 2. (d) Lee, V. Y.; Sekiguchi, A. In *Reviews of Reactive Intermediate Chemistry*; Platz, M. S.; Moss, R. A.; Jones, M., Jr., Eds.; John Wiley & Sons: Hoboken, NJ, 2004. (e) Curran, D. P. *Adrichimica Acta* **2000**, *33*, 104. (f) Curran, D. P. *Synthesis* **1988**, 417. (g) Barton, D. H. R.; Ozbalik, N. *J. Chin. Chem. Soc.* **1988**, *35*, 247. (h) Giese, B. *Angew. Chem.* 1985, *97*, 555; *Angew. Chem., Int. Ed. Engl.*, 1985, *24*, 553.

(10) Frisch, M. J.; Trucks, G. W.; Schlegel, H. B.; Scuseria, G. E.; Robb, M. A.; Cheeseman, J. R.; Montgomery, Jr., J. A.; Vreven, T.; Kudin, K. N.; Burant, J. C.; Millam, J. M.; Iyengar, S. S.; Tomasi, J.; Barone, V.; Mennucci, B.; Cossi, M.; Scalmani, G.; Rega, N.; Petersson, G. A.; Nakatsuji, H.; Hada, M.; Ehara, M.; Toyota, K.; Fukuda, R.; Hasegawa, J.; Ishida, M.; Nakajima, T.; Honda, Y.; Kitao, O.; Nakai, H.; Klene, M.; Li, X.; Knox, J. E.; Hratchian, H. P.; Cross, J. B.; Adamo, C.; Jaramillo, J.; Gomperts, R.; Stratmann, R. E.; Yazyev, O.; Austin, A. J.; Cammi, R.; Pomelli, C.; Ochterski, J. W.; Ayala, P. Y.; Morokuma, K.; Voth, G. A.; Salvador, P.; Dannenberg, J. J.; Zakrzewski, V. G.; Dapprich, S.; Daniels, A. D.; Strain, M. C.; Farkas, O.; Malick, D. K.; Rabuck, A. D.; Raghavachari, K.; Foresman, J. B.; Ortiz, J. V.; Cui, Q.; Baboul, A. G.; Clifford, S.; Cioslowski, J.; Stefanov, B.; Liu, G.; Liashenko, A.; Piskorz, P.; Komaromi, I.; Martin, R. L.; Fox, D. J.; Keith, T.; Al-Laham, M. A.; Peng, C. Y.; Nanayakkara, A.; Challacombe, M.; Gill, P. M. W.; Johnson, B.; Chen, W.; Wong, M. W.; Gonzalez, C.; Pople, J. A. *Gaussian 03 Revision B.04*; Gaussian, Inc.: Pittsburgh, PA, 2003.

(11) See for example: (a) Matsubara, H.; Schiesser, C. H. *J. Org. Chem.* **2003**, *68*, 9299. (b) Schiesser, C. H.; Skidmore, M. A. *J. Organomet. Chem.* 1998, *552*, 145. (c) Dakternieks, D.; Herny, D. J.; Schiesser, C. H. *J. Chem. Soc., Perkin Trans.* **1998**, *2*, 591.

(12) Glendening, E. D.; Badenhoop, J. K.; Reed, A. E.; Carpenter, J. E.; Bohmann, J. A.; Morales, C. M.; Weinhold, F. *NBO 5.0*; Theoretical Chemistry Institute: University of Wisconsin, Madison, WI, 2001.

(13) (a) Wille, U. *J. Org. Chem.* **2006**, *71*, 4040. (b) Wille, U.; Dreessen, T. *J. Phys. Chem. A* **2006**, *110*, 2195. (c) Wille, U.; Andropof, J. *Aust. J. Chem.* **2007**, *60*, 420. (d) Wille, U.; Heuger, G.; Jargstorff, C. *J. Org. Chem.* **2008**, *73*, 1413. (e) Kyne, S. H.; Schiesser, C. H.; Matsubara, H. *J. Org. Chem.* **2008**, *73*, 427.
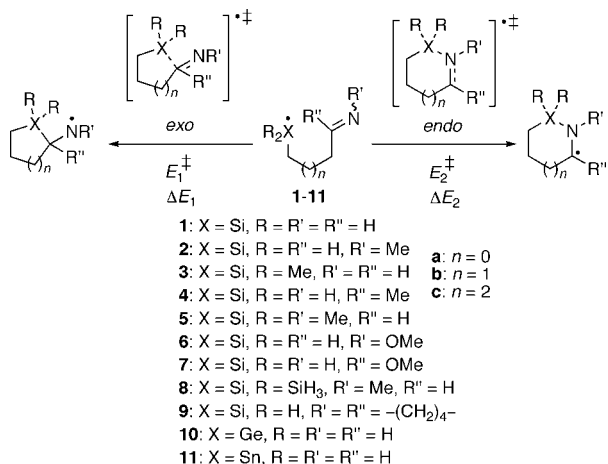
SCHEME 1

1: X = Si, R = R' = R" = H
2: X = Si, R = R" = H, R' = Me
3: X = Si, R = Me, R' = R" = H
4: X = Si, R = R' = H, R" = Me
5: X = Si, R = R' = Me, R" = H
6: X = Si, R = R" = H, R' = OMe
7: X = Si, R = R' = H, R" = OMe
8: X = Si, R = SiH$_3$, R' = Me, R" = H
9: X = Si, R = H, R' = R" = –(CH$_2$)$_4$–
10: X = Ge, R = R' = R" = H
11: X = Sn, R = R' = R" = H

a: n = 0
b: n = 1
c: n = 2

TABLE 1. Activation Energies, $E^{\ddagger}_{1-2}$, Reaction Energies, ΔE_{1-2} (kJ mol^{-1}, with ZPC^a), and Contribution of Orbital Interactions in the *endo* Transition State (%) for Cyclization of Si-, Ge-, and Sn-Radicals onto C=N Double Bonds

		exo pathway		*endo* pathway		orbital interactions in *endo* transition state		
entry	radical	$E^{\ddagger}_1$	ΔE_1	$E^{\ddagger}_2$	ΔE_2	SOMO → π^*	LP$_N$ → SOMO	LP$_N$ → σ^*
1^b	E-1a	62.0	28.5	10.3	−114.8	18	71	11
2^b	Z-1a	61.2	26.7	64.2	−119.7	87	10	3
3^b	E-1b	32.6	−37.0	16.3	−128.3	7	76	17
4^b	Z-1b	34.2	−36.5	38.8	−134.2	71	26	3
5^b	E-1c	40.0	−51.9	30.2	−123.1	39	54	7
6^b	Z-1c	40.6	−53.1	40.0	−105.1	60	36	4
7^b	E-2b	29.0	−45.2	21.3	−113.5	25	65	10
8^b	E-3b	28.6	−48.6	24.0	−146.5	32	56	12
9^b	E-4b	42.5	−19.1	12.8	−123.5	11	74	15
10^b	E-5b	27.7	−55.3	31.3	−128.6	32	60	8
11^b	E-6b	21.9	−77.9	39.5	−77.8	38	57	5
12^b	E-7b	56.6	18.3	34.6	−86.9	26	64	9
13^b	E-8b	31.5	−24.6	21.0	−84.2	29	67	4
14^b	E-9b	34.0	−20.8	5.8	−124.0	25	65	10
15^b	E-10a	66.7	57.1	21.3	−49.8	33	62	5
16^b	E-10b	32.8	−8.7	23.3	−59.9	31	65	4
17^b	E-10c	47.0	−11.4	33.9	−50.4	48	47	5
18^c	E-11a	not possible		15.5	−18.5	67	29	4
19^c	E-11b	40.4	24.2	16.1	−28.3	66	28	6
20^c	E-11c	55.5	24.3	19.5	−24.3	50	42	8

^{a} ZPC = zero-point vibrational energy correction. ^{b} BHandHLYP/6-311G**. ^{c} BHandHLYP/DZP.

earlier observations by us and others.[13] The results of the benchmarking studies (Table S1) and optimized geometries and energies (Gaussian Archive entries) for all ground and transition state structures in this work are available as Supporting Information.

Results and Discussion

Radical Cyclizations onto the Imine C=N Double Bond. We began this investigation by studying the cyclization of Si-radicals into the carbon and nitrogen end of the *E* and *Z* configured imine C=N double bond in compounds **1–9**, which are possessing different chain length and degree of substitution at the radical center and the π system (Scheme 1).

The potential surface for the cyclization onto the carbon end (*exo* pathway) and the nitrogen end (*endo* pathway) was examined, and the results are compiled in Table 1. All tables in this work show the energy values with zero-point vibrational energy correction (ZPC). For the noncorrected relative energies and imaginary frequencies of all transition states, see Supporting Information.

a. Influence of Ring Size and Geometry in Si-Radical Cyclizations. Cyclization of the Si-radical onto the *E* configured C=N double bond in *E*-**1a**–**c** shows a large kinetic and thermodynamic preference for the *endo* pathway with calculated activation energies, $E^{\ddagger}_2$, of 10.3, 16.3, and 30.2 kJ mol^{-1} for the 5-*endo*, 6-*endo*, and 7-*endo* cyclizations, respectively (entries 1, 3, and 5). The competing *exo* cyclizations have higher energy barriers, $E^{\ddagger}_1$, by ca. 50 kJ mol^{-1} (4-*exo*), 16 kJ mol^{-1} (5-*exo*), and 10 kJ mol^{-1} (6-*exo*), with the 4-*exo* process even being endothermic.

In contrast to this, the *exo* pathway is kinetically preferred in the cyclization of the Si-radical onto the *Z* configured C=N double bond in *Z*-**1a** and *Z*-**1b**, whereas in *Z*-**1c** $E^{\ddagger}_1$ and $E^{\ddagger}_2$ for the competing 6-*exo* and 7-*endo* processes are practically identical (entries 2, 4, and 6). Inspection of the results from the NBO analysis of the respective *endo* transition states, which are also given in Table 1, revealed that in the case of *E*-**1a**–**c** multiple orbital interactions are occurring, with interactions of the lone pair at nitrogen with the SOMO and LUMO at the radical center, e.g., LP$_N$ → SOMO and LP$_N$ → σ^*, comprising together 82% (*E*-**1a**), 93% (*E*-**1b**), and 61% (*E*-**1c**) of the total orbital interactions, thus rendering the "classical" SOMO → π^* interaction of the nucleophilic radical with the π bond only a minor contributor.[14,15] The situation is reversed in the case of *Z*-**1a**–**c**, where LP$_N$ interactions with the radical center in the respective *endo* transition states are small compared with the SOMO → π^* interactions that comprise 87% (*Z*-**1a**), 71% (*Z*-**1b**), and 60% (*Z*-**1c**) of the total interactions. The lower contribution of LP$_N$ interactions in these transition states leads to a significant increase of $E^{\ddagger}_2$ for the *endo* pathway, compared with the cyclizations of *E*-**1a**–**c**, whereas $E^{\ddagger}_1$ for the *exo* pathway is largely unaffected.

Figure 2 shows the optimized transition state geometries for the *endo* cyclizations of *E*-**1a**–**c** and *Z*-**1b**.

The dominating LP$_N$ interactions with the radical center in the 6-*endo* transition state of *E*-**1b** (Figure 2b) lead to an apparently sideways attack of the Si-radical at N, essentially in plane with the π-system. This nearly coplanar arrangement can be conveniently described by the tetrahedral angle between the radical center and the π system, $\theta_{Si-N-C-H}$, which is 166° in this transition state. The orbital occupying the LP$_N$ is ideally aligned for interaction with both the SOMO and σ^* orbital (not shown) at the radical center. The LP$_N$ → σ^* interaction leads to a weakening (elongation) of the respective Si−H′ bond, $r_{Si-H'}$, compared to the Si−H″ bond, whose σ^* orbital is not involved. The motion vector at Si reveals that the silyl unit is "leaning back", as is apparent from the wide angle spanned between the H′−Si bond and the imine nitrogen, $\alpha_{H'-Si-N}$, of around 161°, in order to maximize this interaction. Thus, the 6-*endo* cyclization of *E*-**1b** is principally not a radical cyclization but should rather be regarded as a nucleophilic addition to the radical center, which is "observed" by the unpaired electron. In contrast to this, in the 6-*endo* transition state for the cyclization of *Z*-**1b** (Figure 2d), the LP$_N$ points away from the radical center so that only a poor interaction is possible. In this case, the radical attack occurs perpendicular to the π-system ($\theta_{Si-N-C-H}$ ca.

(14) NBO analyses for all transition states to the carbon end of the π systems revealed only SOMO → π^* interactions.

(15) In order to facilitate comparison between the various radical cyclizations studied in this work, the contributions of the different orbital interactions in the transition state are given as percentage. The NBO energies in kJ mol^{-1} are available in Supporting Information.
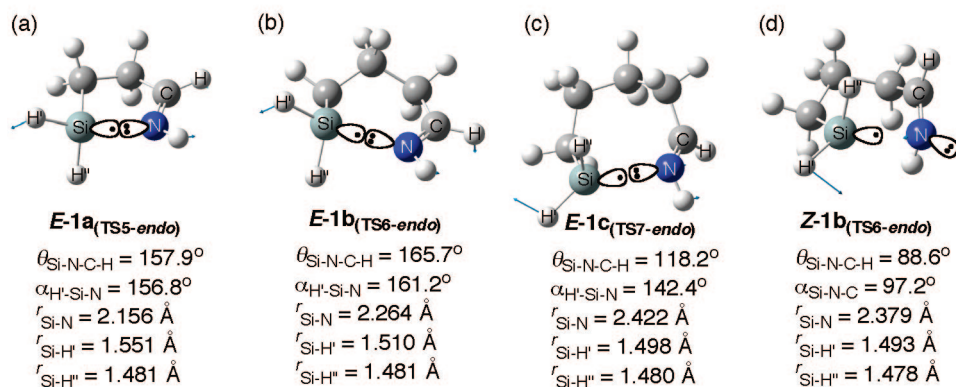
FIGURE 2. Optimized geometries of the transition states, selected dihedral angles (θ), angles (α), distances (r), and motion vectors (blue arrows) for the *endo* cyclization of (a) *E*-1a, (b) *E*-1b, (c) *E*-1c, and (d) *Z*-1b (BHandHLYP/6-311G**). For clarity, only the SOMO and LP$_N$ are shown.

89°), and there is no unusual motion in this transition state. The similarity with a "classical" radical addition transition state is also apparent from the nearly tetrahedral angle of radical attack at nitrogen, α_{Si-N-C}, of 97°.

Because of increased ring strain in the transition states for both the 5-*endo* and the 7-*endo* cyclizations of *E*-1a and *E*-1c, respectively (Figure 2a,c), the radical center, LP$_N$ and π system form a slightly distorted plane.[16] As a consequence, LP$_N$ interactions with the radical center should be smaller and SOMO $\rightarrow \pi$* interactions should be increased in these two transition states, compared with the 6-*endo* cyclization of *E*-1b, which is exactly what we observed (Table 1, entries 1 and 5).

As expected, with increasing ring size of the *endo* transition state, the distance between the radical center and N, r_{Si-N}, increases from 2.156 Å in *E*-1a to 2.422 Å in *E*-1c (Figure 2a–c). It is quite remarkable, however, that the 6-*endo* transition state of *E*-1b, which is dominated by LP$_N \rightarrow$ SOMO and LP$_N \rightarrow \sigma$* interactions, has a ca. 5% shorter Si–N distance than the 6-*endo* transition state of *Z*-1b, which is predominantly governed by SOMO $\rightarrow \pi$* interactions (Figure 2b,d).

b. Influence of Substitution in Si-Radical Cyclizations. From the previous results it appears that LP$_N$ interactions with the radical center are at maximum in six-membered transition states. Therefore, using the competing 5-*exo* and 6-*endo* pathways in Si-radical cyclizations onto *E*-configured imines *E*-2b–*E*-9b, we next investigated the influence of substituents at Si and on both sites of the imine π system on LP$_N$ interactions with the radical center in the 6-*endo* transition state (see Table 1 and Figure 3).

Although the 6-*endo* transition states in all of the investigated systems *E*-2b–*E*-9b showed the unusual motion arising from multicomponent orbital interactions, the substitution pattern clearly influenced the extent of LP$_N$ interactions with the radical center. Methyl groups at the imine nitrogen (*E*-2b, entry 7), at Si (*E*-3b, entry 8), or on both Si and N (*E*-5b, entry 10) increase $E^{\ddagger}_2$ for the *endo* pathway by ca. 5–16 kJ mol^{-1} with lowering $E^{\ddagger}_1$ for the *exo* cyclization at the same time by ca. 4–5 kJ mol^{-1}, compared to the unsubstituted parent system *E*-1b. Nevertheless, the *endo* cyclization onto N is still the kinetically and thermodynamically more favorable pathway. NBO analysis revealed

(16) See, for example: (a) Rao, K. A. N. *J. Chem. Soc.* **1929**, 1954. (b) Bach, R. D.; Dmitrenko, O. *J. Am. Chem. Soc.* **2006**, *128*, 4598. (c) Khoury, P. R.; Goddard, J. D.; Tam, W. *Tetrahedron* **2004**, *60*, 8103. (d) Qudrat-I-Khuda, M. *Nature* **1933**, *132*, 210. (e) Thakur, R. S. *J. Chem. Soc.* **1932**, 2120.

that the increased barrier $E^{\ddagger}_2$ for the *endo* cyclization of *E*-2b, *E*-3b, and *E*-5b is due to a reduction of the LP$_N$ interaction with the radical center in the transition state to 75% and 68%, respectively, of the total orbital interactions. This could be due to a shift of orbital energies at Si or N caused by the methyl groups and/or increased steric hindrance at the radical center or at the π system, respectively. Geometrically, the increased SOMO $\rightarrow \pi$* interactions in these *endo* transition states lead to a less coplanar arrangement between the radical center and the imine moiety, as is apparent from the smaller dihedral angle $\theta_{Si-N-C-H}$ (Figure 3a,b,d), compared to that in *E*-1b (Figure 2b). On the other hand, a methyl substituent at the imine carbon (*E*-4b, entry 9) lowers $E^{\ddagger}_2$ for the *endo* cyclization to only 12.8 kJ mol^{-1}, whereas $E^{\ddagger}_1$ for the *exo* cyclization is increased to 42.5 kJ mol^{-1}. This suggests that electron-donating substituents at the π system α to the reaction site increase the electron density at N and therefore its nucleophilicity, leading in this case to LP$_N$ interactions with the radical center that are comprising 89% of the total orbital interactions in the *endo* transition state during the cyclization of *E*-4b. A dihedral angle $\theta_{Si-N-C-C'}$ of ca. 153° reflects the coplanar arrangement of radical center and LP$_N$ in order to maximize this interaction (Figure 3c). On the other hand, the increased steric hindrance on the imine carbon leads to a disfavored 5-*exo* cyclization pathway for *E*-4b.

The effect of methoxy substituents at the C=N double bond on the regiochemistry of Si-radical cyclizations is quite remarkable. A methoxy group at N in *E*-6b renders the *endo* pathway kinetically unfavorable with $E^{\ddagger}_2$ being ca. 18 kJ mol^{-1} higher than $E^{\ddagger}_1$ (entry 11). This finding cannot be solely attributed to an increased steric hindrance at N, especially since the N-methylated compounds *E*-2b and *E*-5b mentioned above are preferably cyclizing in an *endo* fashion. NBO analysis reveals a contribution of LP$_N$ interactions with Si of only 62% in the *endo* transition state in *E*-6b, suggesting that the electronegativity of oxygen lowers the electron density at N and therefore its nucleophilicity through inductive effects. The reduced LP$_N$ interaction in the 6-*endo* transition state is also obvious from its geometry, where the dihedral angle $\theta_{Si-N-C-H}$ of ca. 134° indicates a barely coplanar arrangement of radical center and π system (Figure 3e). On the other hand, a methoxy substituent on the imine carbon (*E*-7b, entry 12) leads to a preferred *endo* cyclization mode, whereas the *exo* cyclization pathway is both kinetically and thermodynamically disfavored. In this case, the predicted
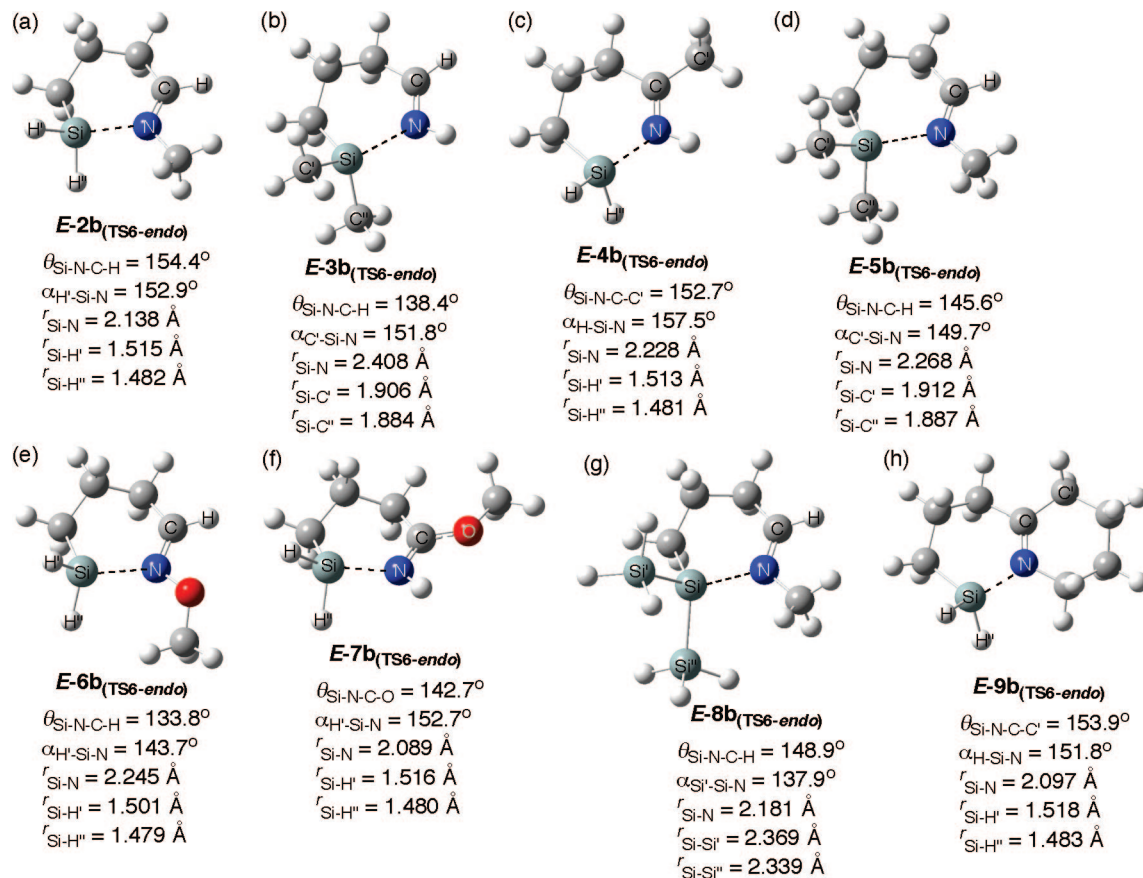
FIGURE 3. Optimized geometries of the 6-*endo* transition states, selected dihedral angles (θ), angles (α) and distances (r) in the cyclization of (a) **E-2b**, (b) **E-3b**, (c) **E-4b**, (d) **E-5b**, (e) **E-6b**, (f) **E-7b**, (g) **E-8b**, and (h) **E-9b** (BHandHLYP/6-311G**).

endo selectivity suggests that the lone pairs at oxygen act as electron donor by increasing the electron density of the double bond, and therefore ultimately also at N, through resonance effects. This is manifested by LP_N interactions with the radical center contributing 73% to the total orbital interactions and a more coplanar arrangement between π system and Si ($\theta_{Si-N-C-H}$ ca. 143°) in the *endo* transition state (Figure 3f).

Finally, the calculations show that, like methyl groups, silyl substituents at the Si-radical center (**E-8b**, entry 13) do not affect the regiochemistry of the radical cyclizations significantly, compared with the unsubstituted parent system **E-1b**. Interestingly, when the *E*-configuration at the imine double bond is frozen as in the cyclic imine **E-9b** (entry 14), the *endo* cyclization proceeds with a very low $E^{\ddagger}_2$ of only 5.8 kJ mol^{-1}, whereas $E^{\ddagger}_1$ for the *exo* pathway is higher by ca. 28 kJ mol^{-1}. The preferred *endo* cyclization pathways of both **E-8b** (Figure 3g) and **E-9b** (Figure 3h) are clearly governed by LP_N interactions with the radical center in the transition state, which comprise 71% and 75%, respectively, of the total orbital interactions. The computational study of the behavior of **E-8b** and **E-9b** in radical cyclizations has provided useful guidelines for the design of suitable radicals for the experimental verification of the computational predictions, which are currently ongoing in our laboratory.

c. Influence of Ring Size in Ge- and Sn-Radical Cyclizations. In order to explore whether multiple orbital interactions are a phenomenon restricted to only few selected radicals, we investigated the cyclization of Ge- and Sn-centered radicals onto the *E*-configured C=N double bonds in **E-10a−c** and **E-11a−c**, respectively (see Scheme 1).

We were indeed pleased to realize that Ge-radicals are cyclizing with large kinetic preference in an *endo* fashion to the nitrogen end of the imine (entries 15−17). However, the computed values for $E^{\ddagger}_2$ are higher by up to 10 kJ mol^{-1}, compared to those for the respective Si-radicals **E-1a−c**. NBO analysis revealed LP_N interactions with the radical center in the respective *endo* transition states comprising 67% (**E-10a**), 69% (**E-10b**), and 52% (**E-10c**), respectively, of the total orbital interactions. On the other hand, $E^{\ddagger}_1$ for the competing *exo* pathway is higher in energy by 10−42 kJ mol^{-1}, depending on the ring size, with the 4-*exo* cyclization being significantly endothermic.

Similar to the smaller main group IV elements studied in this work, also Sn-radicals **E-11a−c** cyclize onto *E*-configured imine C=N bonds with large kinetic and thermodynamic preference in a 5-, 6-, and 7-*endo* fashion, respectively, whereas the competing 5-*exo* (in **E-11b**) and 6-*exo* (in **E-11c**) pathways are both endothermic (entries 18−20). In the case of **E-11a** we were not able to locate both transition state for the 4-*exo* pathway and a stable ground-state geometry of the 4-*exo* product (entry 18). NBO analyses of the respective *endo* transition states revealed again a significant contribution of LP_N interactions with the radical center, comprising 33% (5-*endo*), 34% (6-*endo*) and 50% (7-*endo*) of the total orbital interactions. This contrasts the finding for the analog Si-radicals, where a maximum of $LP_N \rightarrow$ SOMO and $LP_N \rightarrow \sigma^*$ interactions was found in six membered transition states (see entries 1, 3, and 5). We suggest that this different outcome is due to the larger size of Sn, which allows a proper
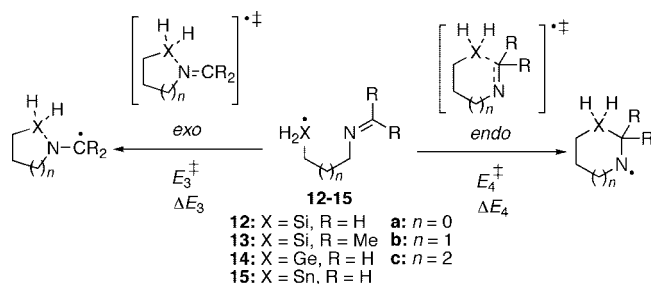
SCHEME 2

12: X = Si, R = H   **a**: n = 0
13: X = Si, R = Me   **b**: n = 1
14: X = Ge, R = H   **c**: n = 2
15: X = Sn, R = H

TABLE 2. Activation Energies, $E^{\ddagger}_{3-4}$, Reaction Energies, ΔE_{3-4} (kJ mol^{-1}, with ZPC), and Contribution of Orbital Interactions in the *exo* Transition State (%) for Cyclization of Si-, Ge-, and Sn-Radicals onto N=C Double Bonds

		exo pathway		*endo* pathway		orbital interactions in *exo* transition state		
entry	radical	$E^{\ddagger}_3$	ΔE_3	$E^{\ddagger}_4$	ΔE_4	SOMO → π^*	LP$_N$ → SOMO	LP$_N$ → σ^*
1[a]	12a	35.9	−57.8	36.5	−57.7	37	56	7
2[a]	12b	13.1	−120.0	36.4	−66.4	22	67	11
3[a]	12c	15.5	−127.3	31.1	−65.2	2	86	12
4[a]	13b	7.7	−98.0	39.2	−36.2	22	68	10
5[a]	13c	22.5	−96.7	48.1	−28.2	27	66	7
6[a]	14a	54.0	13.7	38.2	−23.7	58	40	2
7[a]	14b	28.6	−51.1	37.0	−31.1	39	56	5
8[a]	14c	30.3	−58.0	32.1	−32.2	2	89	9
9[b]	15a	53.6	38.0	39.9	12.8	94	5	1
10[b]	15b	26.7	−18.1	38.5	2.8	72	24	4
11[b]	15c	18.4	−34.0	24.8	−11.3	72	24	4

[a] BHandHLYP/6-311G**. [b] BHandHLYP/DZP.

alignment of radical center and LP$_N$ only in transition states with larger ring size.

Generally, the extent of LP$_N$ interactions with the radical center in the *endo* transition states of Ge- and Sn-radical cyclizations onto *E* configured C=N double bonds are smaller, compared to those in the analog Si-radical cyclizations. This may be due to slightly different orbital energies at Ge and Sn, leading to reduced LP$_N$ → radical center interactions. The geometries of the respective *endo* transition states of Ge- and Sn-radicals *E*-10a−c and *E*-11a−c, respectively, are very similar to those of the Si-radical cyclizations *E*-1a−c (see Figure 2a−c) and are given in Figure 7 in Supporting Information.

Radical Cyclizations onto the Imine N=C Double Bond. Since multiple orbital interactions are clearly governing the regioselectivity of Si-radical cyclizations onto imine E configured C=N bonds, we next investigated the cyclization onto imines possessing the alternative regiochemistry, e.g., an N=C double bond. In this case, cyclization onto nitrogen proceeds in *exo* fashion. The systems studied, which are shown in Scheme 2, varied in both chain length and substitution at the sp^2 carbon. Table 2 compiles the results of the computations.

The data show that only in the case of the Si-radical with the shortest chain, e.g., **12a**, the 4-*exo* and 5-*endo* pathways are competing processes with $E^{\ddagger}_3$ and $E^{\ddagger}_4$ being only 0.6 kJ mol^{-1} apart (entry 1). Cyclization of the higher homologues **12b/c** and **13b/c** proceeds with significantly lower $E^{\ddagger}_3$ to give the respective *exo* products, which are also thermodynamically preferred. This is in sharp contrast to the cyclizations onto the C=N double bond (see Table 1), where the *endo* products are generally thermodynamically favored. For the 4-*exo* transition state during the cyclization of **12a**, NBO analysis revealed a

comparably moderate LP$_N$ interaction with the radical center comprising 63% of the total orbital interactions. The combined LP$_N$ → SOMO and LP$_N$ → σ^* interactions increase to 78% in the 5-*exo* cyclization of **12b** and reach a maximum of 98% in the six-membered transition state of the 6-*exo* cyclization of **12c**. Thus, the latter cyclization has virtually no radical character at all! Figure 4a−c shows exemplary the optimized 4-, 5-, and 6-*exo* transition state geometries for the cyclization of **12a−c**. As before, the dominating nucleophilic attack of LP$_N$ at the radical center leads to a coplanar arrangement between Si and π system, with a dihedral angle $\theta_{Si-N-C-H}$ ranging from 134° (**12a**) to 159° (**12c**), and the well-known "leaning-back" movement of the radical center, which is illustrated by the wide angle $\alpha_{H'-Si-N}$ of 151−157°, in order to maximize the various orbital interactions. Also in these cases, the LP$_N$ → σ^* interaction leads to an elongation of the respective Si−H bond, $r_{Si-H'}$, compared to the Si−H″ bond, whose σ^* orbital is not involved.

To further illustrate the geometrical impact of these LP$_N$ interactions with the radical center, the 5-*exo* transition state geometry of **E-1b** is exemplary shown in Figure 4d (see also Table 1, entry 3). This cyclization is exclusively controlled by SOMO → π^* interactions and proceeds in a "classical" fashion with the radical attacking the π system with a nearly tetrahedral angle (α_{Si-C-N} ca. 97°).[2]

The cyclizations of Ge- and Sn-radicals onto the N=C bond are also governed by multiple orbital interactions. As was already observed before, however, especially for Sn-radicals but also with Ge-radicals, the extent of LP$_N$ interactions with the radical center is generally less pronounced compared to those of Si-radicals, which may be due to the larger size and different orbital energies at Ge and Sn. The 4-*exo* pathways are kinetically and thermodynamically less favorable for both **14a** and **15a** than the respective 5-*endo* pathways (entries 6 and 9). With the larger homologues **14b,c** and **15b,c**, respectively, the cyclizations are predicted to proceed preferentially in an *exo* fashion (entries 7, 8 and 10, 11), which is, according to NBO analyses, again due to LP$_N$ interactions with Ge or Sn in the respective *exo* transition states. A drastic case is the 6-*exo* cyclization in **14c**, where LP$_N$ interactions with Ge comprise 98% of the total orbital interactions in the transition state, suggesting that this is formally no radical reaction at all. Selected geometrical parameters for the respective transition states for the *exo* cyclization of **14a−c** and **15a−c** are given in Figure 8 in Supporting Information.

Radical Additions and Cyclizations onto the Nitrile C≡N Triple Bond. Can the lone pair at nitrogen in nitriles, which is accommodated in an sp orbital and therefore less nucleophilic than a lone pair in an sp^2 orbital, also become involved in orbital interactions during addition of Si-, Ge- and Sn-centered radicals to the C≡N triple bond? As a first step in the exploration of multicomponent interactions in radical additions to nitriles, we studied the potential surface for the *inter*molecular addition of H$_3$Si•, H$_3$Ge• and H$_3$Sn• to the C end (*C*-philic) and N end (*N*-philic) of the C≡N triple bond in acetonitrile (Scheme 3a). The results are compiled in Table 3.

The computations reveal that this reaction, which proceeds via initial formation of an acetonitrile/radical association complex (not shown), is only in the case of H$_3$Si• exothermic for both the *C*-philic (ΔE_5 ca. −36 kJ mol^{-1}) and *N*-philic (ΔE_6 ca. −52 kJ mol^{-1}) addition (entry 1). The *N*-philic addition of H$_3$Si• has an only 1.7 kJ mol^{-1} lower activation barrier, $E^{\ddagger}_6$, than the competing *C*-philic pathway ($E^{\ddagger}_5$). For the *N*-philic
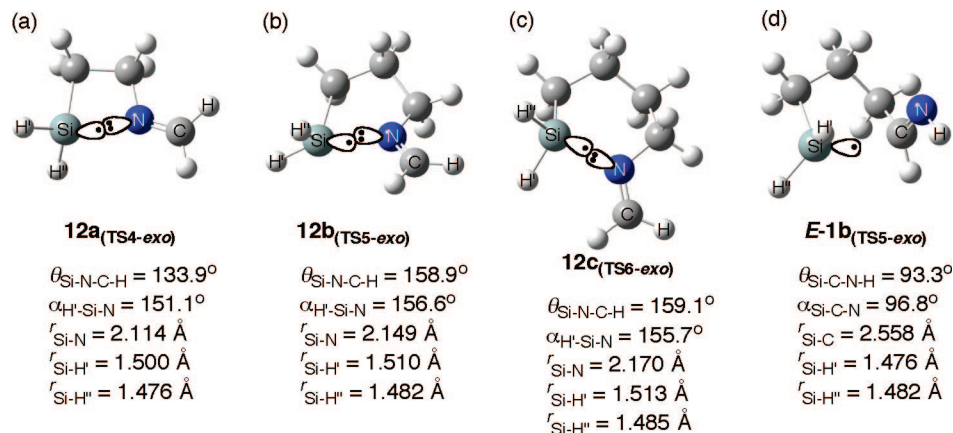
FIGURE 4. Optimized geometries of the transition states, selected dihedral angles (θ), angles (α), and distances (r) for the *exo* cyclization of (a) **12a**, (b) **12b**, (c) **12c**, and (d) **E-1b** (BHandHLYP/6-311G**). For clarity, only the SOMO and LP_N (where required) are shown.
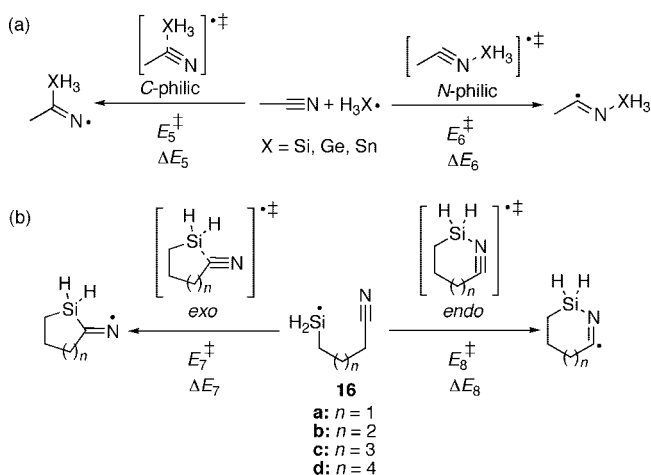
SCHEME 3

TABLE 3. Activation Energies, $E^{\ddagger}_{5-6}$, Reaction Energies, ΔE_{5-6} (kJ mol^{-1}, with ZPC), and Contribution of Orbital Interactions in the *N*-philic Transition State (%) for Addition of H$_3$Si•, H$_3$Ge•, and H$_3$Sn• to the C≡N Triple Bond in Acetonitrile[a]

		C-philic pathway		N-philic pathway		orbital interactions in N-philic transition state		
						SOMO → π^*	LP_N → SOMO	LP_N → σ^*
entry	X	$E^{\ddagger}_5$	ΔE_5	$E^{\ddagger}_6$	ΔE_6			
1[b]	Si	43.6	−36.1	41.9	−51.8	35	58	7
2[b]	Ge	46.7	−3.5	53.1	11.1	54	41	5
3[c]	Sn	54.5	29.3	80.2	35.1	64	29	7

[a] Via association complex (see text). [b] BHandHLYP/6-311G**. [c] BHandHLYP/DZP.

TABLE 4. Activation Energies, $E^{\ddagger}_{7-8}$, Reaction Energies, ΔE_{7-8} (kJ mol^{-1}, with ZPC), and Contribution of Orbital Interactions in the *endo* Transition State (%) for Cyclization of Si-Radicals onto C≡N Triple Bonds (BHandHLYP/6-311G**)

		exo pathway		endo pathway		orbital interactions in endo transition state		
						SOMO → π^*	LP_N → SOMO	LP_N → σ^*
entry	radical	$E^{\ddagger}_7$	ΔE_7	$E^{\ddagger}_8$	ΔE_8			
1	**16a**	44.8	−26.2	59.9	−38.0	68	32	0
2	**16b**	49.0	−39.5	64.9	−35.1	61	37	2
3	**16c**	64.0	−20.3	70.1	−27.4	57	41	2
4	**16d**	67.4	−16.9	81.0	−8.0	58	40	2

pathway, NBO analysis reveals a combined contribution of 65% of LP_N → SOMO and LP_N → σ^* interactions in the transition state. In the case of H$_3$Ge• addition to acetonitrile, the *N*-philic pathway becomes both kinetically and thermodynamically unfavorable, and this addition should proceed exclusively via the *C*-philic pathway (entry 2). Finally, the addition of H$_3$Sn• to acetonitrile shows high activation barriers, especially for the *N*-philic radical attack (entry 3). Since both addition pathways are also significantly endothermic, addition of H$_3$Sn• to acetonitrile should not occur at all. However, NBO analyses of the *N*-philic transition state in both the H$_3$Ge• and H$_3$Sn• addition reveal LP_N interactions with the radical center comprising 46% and 36% of the total orbital contributions, respectively, which are apparently too minor to render this pathway at least

kinetically favorable. Selected geometrical parameters of the respective *N*-philic transition states are given in Figure 9 in Supporting Information.

Because the *N*-philic pathway in the addition of Ge- and Sn-centered radicals onto nitriles is kinetically disfavored, the radical cyclization onto the C≡N triple bond was only studied with the Si-centered radicals **16a–d** (Scheme 3b). The computations revealed (Table 4) that these cyclizations occur with significant *exo* preference in all cases, with the activation barrier $E^{\ddagger}_8$ for the respective *endo* pathways being higher by 6−15 kJ mol^{-1}, depending on the ring size. Kinetically, the 5-*exo* and 6-*exo* cyclization of **16a** and **16b**, respectively (entries 1 and 2), are the most favorable processes, whereas cyclizations to the larger seven [7-*exo* (**16c**)/7-*endo* (**16b**)], eight [8-*exo* (**16d**)/8-*endo* (**16c**)] or nine membered rings [9-*endo* (**16d**)] show increasing activation barriers $E^{\ddagger}_7$ and $E^{\ddagger}_8$. Thermodynamically, however, both *exo* and *endo* cyclizations are feasible processes for all ring sizes, although these cyclizations are generally less exothermic compared with the cyclizations of Si-radicals onto C=N double bonds, which may be explained by the higher energy of the vinyl radicals formed in radical additions to nitriles.[2]

NBO analysis of all *endo* transition states revealed that the "classical" SOMO → π^* interaction is the major interaction in all cases, which decreases slightly from 68% to ca. 58% with increasing ring size. At the same time the total LP_N interactions with the radical center are gradually increasing from 32% to ca. 43%. The optimized geometries for these four transition states, shown in Figure 5, reveal the origin of this finding.

In the 6-*endo* transition state in the cyclization of **16a**, ring strain induced by the triple bond causes the LP at nitrogen to be perpendicular to the trajectory of radical attack. With increasing ring size and flexibility of the carbon framework,
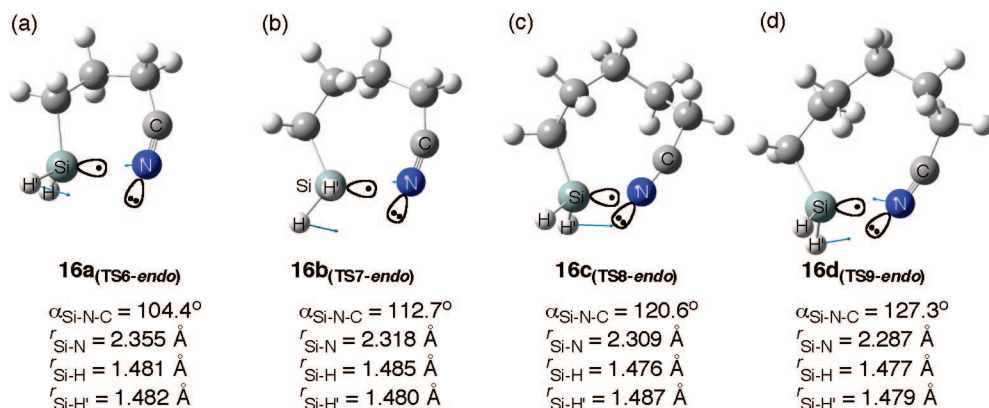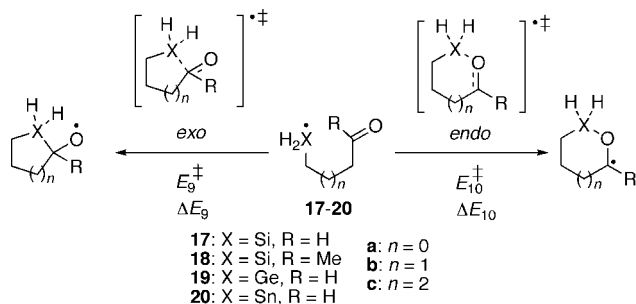
FIGURE 5. Optimized geometries of the transition states, selected angles (α), distances (r), and motion vectors (blue arrows) for the *endo* cyclization of of (a) **16a**, (b) **16b**, (c) **16c**, and (d) **16d** (BHandHLYP/6-311G**). For clarity, only the SOMO and LP$_N$ are shown.

SCHEME 4

LP$_N$ interactions with the radical center become geometrically more feasible. These interactions can be visualized by α_{Si-N-C} representing the angle of radical attack at the π system, which increases from ca. 104° in the most strained (**16a**) to ca. 127° in the largest system (**16d**). The increasing contribution of LP$_N$ interactions with the radical center leads to shortening of the distance between the silyl unit and nitrogen, r_{Si-N}, in these transition states, similar to the finding in radical cyclizations onto imines described above. In principle, a better alignment of LP$_N$ and radical center would be expected during the *endo* cyclization of higher homologues of **16d**, but the increasing transannular ring strain that builds up in this process will render such cyclizations entropically unfavorable,[2] which is why we refrained from studying systems larger than **16d**.

Radical Cyclizations onto the Carbonyl C=O Double Bond. Finally, we investigated the cyclization of Si-, Ge-, and Sn-centered radicals onto carbonyl C=O double bonds (Scheme 4). Since oxygen is more electronegative than nitrogen, the lone pairs at oxygen are less nucleophilic, and we were therefore curious to what extent this may affect LP$_O$ interactions with the radical center in the *endo* transition state during cyclizations onto the carbonyl oxygen. The results of the computations are compiled in Table 5.

It is quite apparent that LP interactions with the radical center are generally reduced during cyclizations onto the carbonyl oxygen, compared to cyclizations onto the imine nitrogen. Using the aldehydes **17** as example, in the 5-*endo* cyclization of **17a** and the 6-*endo* cyclization of **17b** (entries 1 and 2) the LP$_O$ interactions with the radical center comprise 63% and 59%, respectively, compared with 82% and 93% LP$_N$ interactions during the *endo* cyclizations of the respective *E* configured imines **1a** and **1b** (see Table 1, entries 1 and 3). For the 7-*endo* cyclization in **17c**, the LP$_O$ interactions in the transition state are similar to LP$_N$ interactions predicted for the 7-*endo*
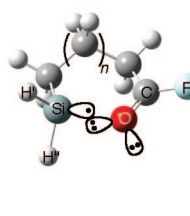
TABLE 5. Activation Energies, $E^{\ddagger}_{9-10}$, Reaction Energies, ΔE_{9-10} (kJ mol^{-1}, with ZPC), and Contribution of Orbital Interactions in the *endo* Transition State (%) for cyclization of Si-, Ge-, and Sn-Radicals onto C=O Double Bonds

entry	radical	*exo* pathway $E^{\ddagger}_9$	ΔE_9	*endo* pathway $E^{\ddagger}_{10}$	ΔE_{10}	SOMO → π^*	LP$_O$ → SOMO	LP$_O$ → σ^*
1[a]	**17a**	54.5	54.5	42.9	−102.7	37	56	7
2[a]	**17b**	34.1	−9.5	46.5	−119.6	41	46	13
3[a]	**17c**	40.6	−20.2	49.2	−108.7	34	56	10
4[a]	**18a**	86.1	75.6	39.1	−96.6	37	54	9
5[a]	**18b**	45.7	11.7	43.8	−111.8	44	46	10
6[a]	**18c**	58.5	6.8	46.1	−98.1	34	54	12
7[a]	**19a**	79.3	b	55.8	−24.9	46	50	4
8[a]	**19b**	37.0	17.3	56.8	−35.5	57	39	4
9[a]	**19c**	44.0	11.8	60.0	−26.1	50	48	2
10[c]	**20a**	not possible		48.7	−3.2	81	17	2
11[c]	**20b**	45.9	41.1	49. 4	−14.9	80	17	3
12[c]	**20c**	55.6	41.0	48.7	−9.9	70	25	5

[a] BHandHLYP/6-311G**. [b] Could not be located (see text). [c] BHandHLYP/DZP.

cyclization of **E-1c** (Table 5 entry 3 vs Table 1 entry 5). Thus, the activation energy $E^{\ddagger}_{10}$ for the *endo* cyclization of the Si radical onto the C=O bond in **17a**−**c** are higher by ca. 18− 33 kJ mol^{-1}, compared with the analog cyclizations onto the imine C=N bond in **E-1a**−**c** ($E^{\ddagger}_2$). On the other hand, $E^{\ddagger}_9$ and $E^{\ddagger}_1$ for the respective competing *exo* cyclizations onto the carbon end in C=O or C=N, respectively, are essentially similar (except for the 4-*exo* cyclizations). Only in the case of the smallest system under investigation, e.g., **17a**, *endo* cyclization is the kinetically favored pathway, presumably because ring strain prevents formation of the 4-*exo* product, whereas the larger homologues **17b** (entry 2) and **17c** (entry 3) cyclize preferably in an *exo* fashion to give the thermodynamically less stable products. The additional methyl substituent at the π system in the ketones **18a**−**c** has practically no effect on the extent of LP$_O$ interactions with the radical center and barrier height $E_{10}^{\ddagger}$ in the respective *endo* transition states (entries 4−6). However, because of the increased steric hindrance at C, the activation barrier $E^{\ddagger}_9$ for the competing *exo* cyclization increases by ca. 12−32 kJ mol^{-1}, depending on ring size, making this pathway in all cases kinetically less favorable than the *endo* cyclization.

Cyclizations of Ge- and Sn-centered radicals onto the carbonyl bond follow a similar pattern as was found for their cyclizations onto imine double bonds (see above). Compared with Si-radicals, LP$_O$ interactions with the radical center are

Radical	Transition state	$\theta_{Si-O-C-R}$ /°	$\alpha_{H'-Si-O}$ /°	r_{Si-O} /Å	$r_{Si-H'}$ /Å	$r_{Si-H''}$ /Å
17a	5-*endo*	146.7	148.0	2.111	1.496	1.475
18a	5-*endo*	144.8	148.7	2.048	1.493	1.473
17b	6-*endo*	137.2	146.5	2.146	1.499	1.475
18b	6-*endo*	148.7	146.5	2.093	1.499	1.476
17c	7-*endo*	143.4	148.1	2.170	1.501	1.474
18c	7-*endo*	141.8	148.5	2.113	1.502	1.475

FIGURE 6. Optimized geometries of the transition states, selected angles (α), dihedral angles (θ), and distances (r) for the *endo* cyclization of **17a−c** and **18a−c** (BHandHLYP/6-311G**). For labeling see Scheme 4. For clarity, only the SOMO and LP$_O$ are shown.

generally less important during the *endo* cyclizations of the Ge-radicals **19a−c** (max. 54% in the case of **19a**, entry 7). The *endo* cyclizations of the Sn-centered radicals (**20a−c**) onto C=O are mainly governed by the "classical" SOMO → $\pi*$ interactions (entries 10−12). With Ge- and Sn-radicals, all *exo* pathways under investigation are endothermic; a stable geometry of the 4-*exo* product in the cyclization of **19a** could not be located at the BHandHLYP/6-311G** level of theory (entry 7),[17] and the 4-*exo* cyclization of **20a** appears to be even impossible (entry 10). Thus, the smaller systems **19a** and **20a** can only undergo 5-*endo* cyclization, whereas mixed *exo/endo* selectivities without clear trends are found with the respective larger homologues.

Geometrically, the reduced relevance of LP$_O$ interactions with the radical center in the *endo* transition states of **17a−c** and **18a−c** lead to a smaller dihedral angle $\theta_{Si-O-C-R}$ (Figure 6, with R = H, Me), compared to the analog cyclizations of *E*-**1a−c** (see Figure 2a−c), indicating a less coplanar alignment between the attacking radical and LP$_O$. The reduced demand for optimization of LP$_O$ interactions with Si is also reflected by the less pronounced "leaning back" motion of the silyl unit, resulting in a smaller angle of attack, $\alpha_{H'−Si−O}$. However, the existing LP$_O$ → $\sigma*$ interaction leads to a slight elongation of the respective Si−H′ bond, compared to the Si−H″ bond that is not involved in this interaction.

The geometries of the respective *endo* transition states during the cyclization of the Ge and Sn radicals in **19a−c** and **20a−c** are essentially identical to those of **17a−c** and **18a−c** and are given in Figure 10 in Supporting Information.

Conclusion

This computational study has shown that cyclization of Si-, Ge-, and Sn-centered radicals to the nitrogen end in imine C=N and N=C double bonds occur through simultaneous SOMO → $\pi*$, LP$_N$ → SOMO, and LP$_N$ → $\sigma*$ interactions between the radical center and the π system. These multicomponent orbital interactions are responsible for unusual geometries and motion vectors associated with the transition states involved in these reactions. NBO analyses of the transition states provide quantitative information relating these multicomponent orbital interactions and show that the geometrical availability of the LP at nitrogen has a critical effect on the regioselectivity of these reactions. Cyclization onto the *E* configured C=N double bond in *E*-**1a−c** and *E*-**2b−E**-**9b** proceeds in nearly all cases with high *endo* selectivity to the more electron-rich nitrogen end of the π system, because these reactions are governed by LP$_N$ interactions with the radical center, and SOMO → $\pi*$

interactions are only minor contributors. Drastically spoken, in these cyclizations the role of the unpaired electron can be reduced to being mostly an observer of the nucleophilic attack by nitrogen at the radical center. This shows that the unpaired electron is not necessarily the most reactive site in a radical. On the other hand, in cyclizations onto the *Z* configured C=N double bond in *Z*-**1a−c**, the LP at nitrogen is geometrically not available for interaction with the radical center in the *endo* transition state. Thus, these reactions are predominantly governed by the "classical" SOMO → $\pi*$ interactions and proceed with high *exo* preference to the carbon end of the C=N double bond. The finding that the geometry at the π system regulates the regioselectivity of the radical attack is an interesting perspective for synthetic applications.

Of the various radicals studied in this work, the contribution of LP$_N$ interactions with the radical center are the largest in transition states involving Si-radicals. With increasing size of the atom carrying the unpaired electron, the SOMO → $\pi*$ interactions are gradually increasing on the expense of LP$_N$ interactions with the radical center in the transition state. Although LP$_N$ interactions were also found in the case of Sn−radical cyclizations onto the nitrogen end in both C=N and N=C double bonds (compounds *E*-**11a−c** and **15a−c**), a clear judgment of the directing effect of LP$_N$ interactions in the *N*-philic transition states cannot be easily made in all cases, since the competing cyclization onto the carbon end of the π system is often endothermic. However, it generally appears from our computations on radical cyclizations onto the imine π system that pathways with dominating LP$_N$ → SOMO and LP$_N$ → $\sigma*$ interactions in the transition state are also thermodynamically preferred. Ge-radicals (compounds *E*-**10a−c** and **14a−c**) show a behavior in-between that of Si- and Sn-radicals. Although the LP$_N$ contributions in the *N*-philic transition states are generally smaller compared to Si-radical cyclizations, Ge-radicals usually cyclize with preference to the nitrogen end.

The reduced nucleophilicity of nitrogen in nitriles or oxygen in carbonyl compounds has a drastic effect on the regioselectivity of radical cyclizations onto the C≡N triple bond or the C=O double bond, respectively. Although the computations have revealed that LP interactions with the radical center in the respective *N*-or *O*-philic transition states are occurring in all reactions studied in this work, their contributions to the overall orbital interactions are significantly smaller, compared with LP$_N$ interactions in cyclizations onto the imine π systems. Therefore, cyclizations of Si-radicals onto C≡N bonds and of Si-, Ge-, and Sn-radicals onto C=O bonds, respectively, are predominantly governed by the SOMO → $\pi*$ interactions characteristic for nucleophilic radicals, resulting in attack at the less electron rich site in these π systems, e.g. the carbon atom. This shows

---

(17) The product of the 4-*exo* cyclization of **19a** could be located at the UHF/6-311G** level of theory.

that the polarity of a radical is not an intrinsic property, but that it depends on the reaction partner (*radicalophile*) and its electronic properties, whether the radical reacts as a nucleophile or electrophile. We are currently performing experimental studies to verify our computational predictions.

Supporting Information Available: Table S1, extended Tables 1−5 containing the imaginary frequencies for all transition states, relative energies without and with zero-point vibrational energy correction (ZPC) and NBO energies, Figures 6−10, and Gaussian Archive entries for all optimized geometries. This material is available free of charge via the Internet at http://pubs.acs.org.

JO800750A